

An Enhancement Algorithm of Mine Image Based on Adaptive Transmittance and Hierarchical Threshold Function

Yuanbin Wang, Huaying Wu, Yu Duan and Zongshan Li

Abstract—Aiming at the problems of image degradation caused by uneven illumination, dense haze and high noise under the mine environment, an enhancement algorithm of mine image based on adaptive transmittance and hierarchical threshold function is proposed. Firstly, the multiscale decomposition of the mine degradation image is carried out by wavelet transform. The low-frequency image with haze and the high-frequency images with noise are separated. Secondly, the low-frequency image is dehazed. Through adaptive judgment on the position at the edge of the field depth, the transmittance of this position is optimized by minimum filtering, and the optimized transmittance is smoothed by guide filtering, which can retain the image edge details and suppress the generation of white halo blocks. After that, the high-frequency images are denoised by the hierarchical threshold function, and high-frequency wavelet coefficients are estimated in three sections. The adjustment factors are set to select appropriate parameters to suppress the noise with different scales and keep more high-frequency details while the denoising effect is satisfied. Finally, the brightness of the wavelet reconstructed image is equalized in HSI space to obtain the final enhanced image. Experiment results show that the proposed approach can suppress the noise and haze and enhance image details. Meanwhile, compared with the dark channel prior algorithm, the running efficiency is also improved effectively.

Index Terms—image enhancement, adaptive transmittance, image dehazing, threshold denoise

I. INTRODUCTION

With the continuous development of the coal mining industry, the mine video surveillance system has played an essential role in the safety production of coal mining enterprises and disaster emergency rescue [1-2]. Due to the influences of noise, dense haze, and uneven illumination under the mine environment [3], the image details in the dark area are lost, and halo artifacts exist in the

highlighted area. The scene information under the mine is ambiguous, which affects the image quality collected by the video surveillance system seriously. Therefore, improving mine image quality is significant to mine automation and intelligent mining.

To solve the degradation problem of video surveillance images in mines, there are mainly two methods: image enhancement and image restoration.

(1) Image enhancement-based methods mainly include histogram equalization (HE) [4], wavelet transformation (WT) [5], the Retinex method [6]. HE algorithm can enhance local contrast, but there are some color distortion and partial overexposure in the enhanced image [7]. The WT algorithm has a good denoising effect but does not adjust the low-frequency coefficient, which makes the enhanced image brightness not improve significantly. The Retinex method can improve the image brightness effectively, but the processed image exists color distortion, and halo artifacts are existed due to uneven illumination. Therefore, to overcome these problems, some improved algorithms are employed. Liya Zhang et al. [8] combined the retinex algorithm with bilateral filtering, which can overcome the phenomena of halo artifacts and edge blur. Shoufeng Tang et al. [9] employed an MSR algorithm on the basis of multiscale guided filtering, which can suppress noise and retain edge details. Li et al. [10] proposed the LightenNet for the mapping relationship estimation of low-light images and combined the retinex model to enhance the image brightness. Wei et al. [11] proposed the RetinexNet fully convolutional network, which can improve image contrast effectively. However, it is easy to lose edge details while denoising. The enhancement effect of the above methods is improved significantly, but there are still some problems, such as noise, detail loss and overexposure.

(2) Image restoration-based method. He algorithm [12-13] has a better dehazing effect, but the restored image is dark. Yingjie Mei et al. [14] combined dark channel prior (DCP) algorithm and multiscale retinex for the improvement of image contrast and brightness. However, there was the halo artifact in the restored image. Yong Chen et al. [15] proposed an algorithm combining super pixel segmentation with dark and bright channels to improve the transmittance. Xinyu Zhao et al. [16] proposed a dual-channel prior and illumination map-guided filtering algorithm to refine the transmittance. These methods can avoid residual haze and partial darkness, but there are still halo blocks at the edges. Cai et al. [17] adopted the DehazeNet to learn and estimate the relationship between transmittance and hazy images directly. However, this method is ineffective in restoring the depth of field

Manuscript received June 20, 2022; revised January 11, 2023. This work is supported by the National Natural Science Foundation of China (Grant No. 52174198), Shaanxi Qinchuangyuan (2022KXJ-166), and the National key research and development program of Shaanxi Province, China (2023 YBSF-133).

Yuanbin Wang is an Associate Professor at the College of Electrical and Control Engineering, Xi'an University of Science and Technology, Shaanxi Xi'an 710054, China. (corresponding author phone: +18209280530; e-mail: wangyb998@163.com)

Huaying Wu is a postgraduate at the College of Electrical and Control Engineering, Xi'an University of Science and Technology, Shaanxi Xi'an 710054, China. (e-mail: wuhuaying_1999@126.com)

Yu Duan is a postgraduate at the College of Electrical and Control Engineering, Xi'an University of Science and Technology, Shaanxi Xi'an 710054, China. (e-mail: 307073082@qq.com)

Zongshan Li is an intermediate engineer at the Shaanxi Future Energy Chemical Co., Ltd. Jinjitan Coal Mine, Shaanxi Yulin, China. (e-mail: 174065955@qq.com)

changes, and it is easy to lose edge information. Besides, the algorithm has many parameters, and it is inefficient. Li et al. [18] proposed the AODNet network, in which all parameters were estimated in a unified model. This method can reduce the parameter estimation error and improve computational efficiency significantly. Chen et al. [19] proposed the GCANet network, which restored images without relying on prior knowledge and solved the problem of grid artifacts. But it has high data set requirements and limited application scenarios. The network-based on deep learning can improve the dehazing effect effectively. However, the network structure often fails to consider all haze map features thoroughly, and halo blocks are existed resulting in an incomplete dehazing effect.

Although image quality is improved by the above enhancement methods, the performance of denoising and dehazing cannot be satisfied simultaneously, and image details are lost. To optimize the dehazing and denoising effect, this research mainly conducted two contributions: (1) The adaptive transmittance is proposed at the edge of field depth, which can eliminate halo artifacts and improve the contrast. (2) The hierarchical threshold function is divided into three sections to estimate the wavelet coefficients, which can improve the denoising effect and retain more detail characteristics.

The remainder of this paper is organized as follows. In Section 2, the adaptive transmittance and hierarchical threshold function are described. Then, we mainly introduce the working principle and process of the proposed approach in Section 3. Next, the comparison and analysis of the dehazing, denoising effect, and overall enhancement performance are presented in Section 4, respectively. The conclusion is summarized in Section 5.

II. PROPOSED ALGORITHM

Haze is represented by slow transformation information, mainly concentrated in the low-frequency part after wavelet decomposition [20]. The noise and detailed information in the image are contained in the high-frequency part of the fast transformation. Through comprehensive analysis, the low-frequency component is dehazed by adaptive transmittance, and hierarchical threshold function is employed to denoise high-frequency components. The processing framework is shown in Fig. 1.

A. Adaptive transmittance

The mine environment is full of roadway structures and no

sky domain. Therefore, the dark channel prior (DCP) algorithm is naturally suitable for image dehazing in the mine scene. The low-frequency images are dehazed based on the DCP algorithm [12]. The specific steps of the DCP algorithm are as follows. Firstly, the dark channel is obtained with formula (1). The brightest pixel value of the first 0.1% is taken from the dark channel. Then the highest brightness value of the corresponding point in the original image is selected as atmospheric light value A . The initial transmittance can be obtained with formula (2), and the final low-frequency dehazing image can be obtained with formula (3).

$$j^{dark}(x) = \min_{c \in (r, g, b)} \left(\min_{y \in \varphi(x)} (j^c(y)) \right) \quad (1)$$

$$t_1(x) = 1 - \omega \min_{c \in (r, g, b)} \left[\min_{y \in \varphi(x)} \left[\frac{j^c(y)}{A^c} \right] \right] \quad (2)$$

$$J(x, y) = \frac{I(x, y) - A}{\max(t_1, t_0)} + A \quad (3)$$

Where $j^c(y)$ is a color channel of the image; $\varphi(x)$ is the local area centered at pixel point x ; t_0 is the threshold with the value of 0.1.

He et al. [12] adopted minimum filtering to obtain the dark channel image, so there is a blocky effect at the edge of the field depth, and the restored image is darker overall. The initially estimated transmittance is shown in Fig. 2 (a). He algorithm [13] optimizes the initial transmittance through guide filtering. However, this method does not eliminate the white halo blocks at the edge but dilutes them to the surrounding. The transmittance optimized by guided filtering is shown in Fig. 2 (b).

Aiming at this problem, adaptive transmittance is proposed to eliminate halo blocks. The steps of transmittance optimization are as follows.

(1) The transmittance of minimum filtering $t_2(x)$ is obtained with formula (4), which is the optimized transmittance at the edge of the field depth.

$$t_2(x) = \min_{x \in \varphi(x)} t_1(x) \quad (4)$$

(2) The difference between $t_1(x)$ and $t_2(x)$ can be obtained with formula (5). The position at the edge of the field depth can be judged by the threshold value T with the formula (6).

$$\Delta t = |t_1(x) - t_2(x)| \quad (5)$$

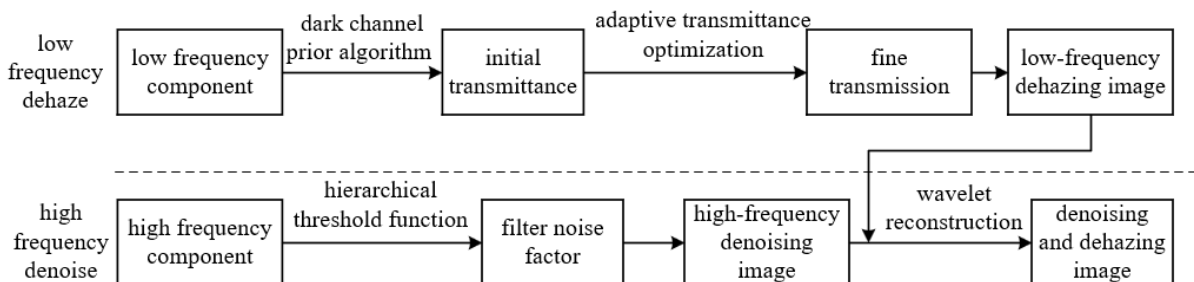


Fig. 1. Processing frame diagram of the low and high-frequency components.

$$T = \frac{\sum_{i=0}^m \sum_{j=0}^n \Delta t}{m \times n} \quad (6)$$

(3) If $\Delta t \geq T$, the transmittance is considered in the edge region of field depth and $t_3(x)$ will be taken as $t_2(x)$. On the contrary, it will be taken as $t_1(x)$. The formula is defined as follows:

$$t_3(x) = \begin{cases} t_2(x), \Delta t \geq T \\ t_1(x), \Delta t < T \end{cases} \quad (7)$$

(4) $t_3(x)$ is smoothed by guided filtering and $t_4(x)$ is the final optimized transmittance. The guide filtering is defined as follows:

$$q_i = a_k I_i + b_k, i \in w_k \quad (8)$$

Where a_k and b_k denote linear parameters of the window w_k ; q_i represents the output pixel value; I_i denotes the pixel value of the guide image.

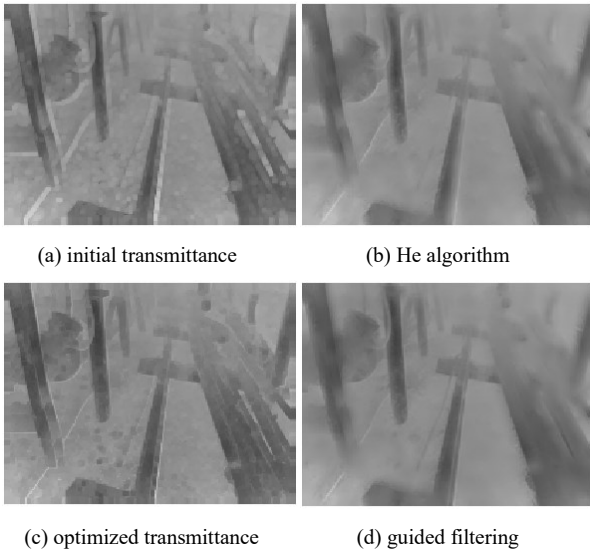


Fig. 2. Comparison of initial transmittance optimization

As can be seen from Fig. 2 (c) and (d), the proposed algorithm can remove white halo blocks in the initial transmittance effectively. Compared with Fig. 2 (c), Fig. 2 (d) shows that the halo block in the detail-rich area is diluted through guided filtering.

B. Hierarchical Threshold Function

Since the denoising performance of the fixed threshold is quite thorough, it is selected to separate the detail component and noise component of high-frequency images preliminarily, which is defined as follows:

$$\lambda = \sigma \sqrt{2 \ln(M \times N)} \quad (9)$$

$$\sigma = \text{meidan}(|\omega_{1,k}|) / 0.6745 \quad (10)$$

Where λ is the fixed threshold, $M \times N$ denotes image size, σ is standard noise variance, and $|\omega_{1,k}|$ represents the first high-frequency coefficients.

Due to the problems of discontinuity and constant deviation of traditional threshold functions, the following threshold functions are proposed in the literature [21] and [22], respectively:

$$\omega_{j,k}^{\wedge} = \begin{cases} \text{sgn}(\omega_{j,k}) \left(|\omega_{j,k}| - 2\lambda / \left(1 + \exp(|\omega_{j,k}| - \lambda) \right) \right), \\ |\omega_{j,k}| \geq \lambda \\ 0, |\omega_{j,k}| < \lambda \end{cases} \quad (11)$$

$$\omega_{j,k}^{\wedge} = \begin{cases} \text{sgn}(\omega_{j,k}) \left(|\omega_{j,k}| - 2\lambda(1-\rho) / \left(1 + \exp(|\omega_{j,k}| - \lambda)^{\rho} \right) \right), \\ |\omega_{j,k}| \geq \lambda \\ \text{sgn}(\omega_{j,k}) \rho \frac{|\omega_{j,k}|^2}{\lambda}, |\omega_{j,k}| < \lambda \end{cases} \quad (12)$$

The asymptotic semi-soft threshold function proposed in the literature [21] can reduce constant deviation. However, it is not flexible enough due to the lack of adjustable factors, and the effect of lowering the deviation is not obvious enough. In the literature [22], the high-frequency coefficients less than the threshold are regarded as a quadratic function without being zeroed directly, which can avoid oscillation caused by direct truncation. However, for the high-frequency coefficient less than the fixed threshold, the threshold function proposed in the literature [22] fails to suppress the noise completely, and the denoising effect is not ideal enough.

Given the problems with the threshold functions mentioned above, the hierarchical threshold function is proposed and defined as:

$$\omega_{j,k}^{\wedge} = \begin{cases} \text{sgn}(\omega_{j,k}) \left(|\omega_{j,k}| - 2\lambda(1-m) / \left(1 + \exp(|\omega_{j,k}| - \lambda)^2 \right) \right), \\ |\omega_{j,k}| \geq \lambda \\ \text{sgn}(\omega_{j,k}) m \frac{|\omega_{j,k}|^2}{\lambda} (|\omega_{j,k}| - \beta\lambda) / (\lambda - \beta\lambda), \beta\lambda \leq |\omega_{j,k}| < \lambda \\ 0, |\omega_{j,k}| < \beta\lambda \end{cases} \quad (13)$$

Where m and β are adjustable parameters within the range of (0,1).

As shown in Fig.3, when the high-frequency coefficients are greater than the fixed threshold, the estimated wavelet coefficient can reduce constant deviation and approach the original wavelet coefficients rapidly. The high-frequency coefficient between $\beta\lambda$ and λ can be improved effectively to protect the edge details of the image. When the high-frequency coefficient is less than $\beta\lambda$, the noise coefficient in the high frequency can be set to 0, which can suppress noise effectively.

The performance of the hierarchical threshold function will be analyzed from the following aspects.

(1) Continuity

$$\lim_{\omega_{j,k} \rightarrow \lambda^+} \omega_{j,k}^{\wedge} = \lim_{\omega_{j,k} \rightarrow \lambda^-} \omega_{j,k}^{\wedge} = \text{sgn}(\omega_{j,k})(m\lambda) \quad (14)$$

Equation (14) indicates the hierarchical threshold function is continuous at λ . In the same way, it's also continuous at $-\lambda$.

$$\lim_{\omega_{j,k} \rightarrow \beta\lambda^+} \omega_{j,k}^{\wedge} = \lim_{\omega_{j,k} \rightarrow \beta\lambda^-} \omega_{j,k}^{\wedge} = 0 \quad (15)$$

Equation (15) shows the hierarchical threshold function is continuous at $\beta\lambda$. It's also continuous at $-\beta\lambda$.

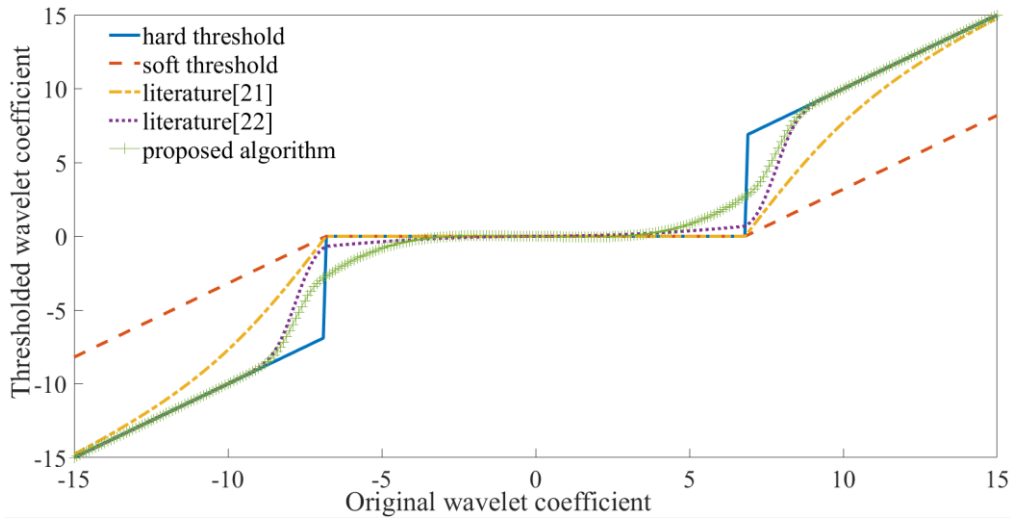


Fig. 3. Threshold function curve

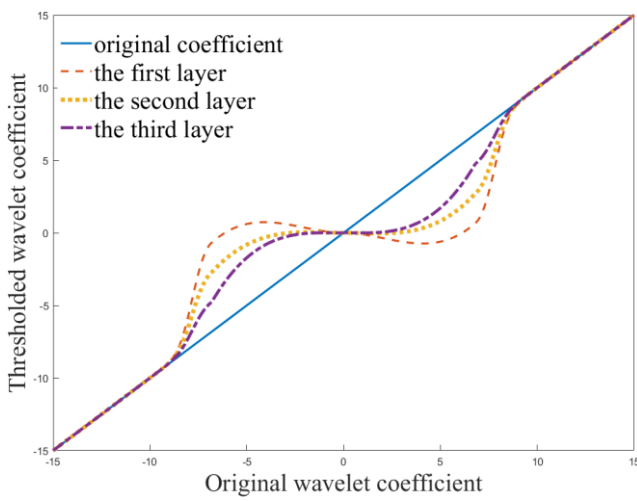


Fig. 4. The adjustment factors of each layer

The pre-estimated wavelet coefficients obtained by the hierarchical threshold function have better continuity, which can avoid oscillation, truncation effect and other visual distortions of the reconstructed image.

(2) Constant deviation

$$\lim_{\omega_{j,k} \rightarrow +\infty} \left(\hat{\omega}_{j,k} - \omega_{j,k} \right) = \lim_{\omega_{j,k} \rightarrow -\infty} \left(\hat{\omega}_{j,k} - \omega_{j,k} \right) = 0 \quad (16)$$

It can be seen from Equation (16) that the constant deviation is eliminated effectively. Compared with the threshold function proposed in the literature [21], the hierarchical threshold function can approach the original wavelet coefficient rapidly, and the image distortion can be avoided.

(3) Adjustment factors m and β

In this paper, noise components are separated by the fixed threshold. The noise components will decrease with the increase of the decomposition scale [23]. Hence, the hierarchical threshold function sets two adjustment factors to keep more detailed components of high-frequency images and compensate for the loss of the effective coefficient caused by the fixed threshold.

When m increases gradually, the wavelet coefficients can be improved effectively, and the image details can be

maintained. When β increases gradually, the denoising effect is more complete. As the number of decomposition layers increases, m will increase and β will decrease.

Fig.4 shows that, with the increase of decomposition layers, the hierarchical threshold function can be closer to the original wavelet coefficient and retain more high-frequency details by adjusting factors. Compared with the threshold function proposed in the literature [22], the hierarchical threshold function is divided into three sections and set two adjustment factors to estimate the wavelet coefficients, which makes the denoising effect more flexible and accurate.

To sum up, by analyzing the continuity, deviation and adjustment factors of the hierarchical threshold function, it is concluded that the proposed method can eliminate deviation and has good continuity and strong flexibility.

III. WORKING PRINCIPLE AND PROCESS

In this paper, the mine image is decomposed by wavelet transform to acquire low-frequency and high-frequency components [24]. Then the coefficients in the low-frequency part are dehazed by adaptive transmittance, and the coefficients in the high-frequency part are denoised by the hierarchical threshold function. Next, the reconstructed enhanced (f_{RE}) image is converted into the HSI space, and the I component is equalized to expand the dynamic range of the pixel gray level while keeping the original H and S components unchanged. Finally, the processed components are converted to RGB space, and the output is the mine enhanced image. The flow chart is presented in Fig. 5.

IV. EXPERIMENTAL RESULTS

Three kinds of experiments are conducted to verify the dehazing, denoising and overall enhancement effect of the proposed algorithm.

For the evaluation of the denoising quality, the peak signal-to-noise ratio (RPSN) is employed and defined as follows:

$$R_{\text{PSN}} = 10 \times \log_{10} \left(\frac{(2^n - 1)^2}{M_{\text{SE}}} \right) \quad (17)$$

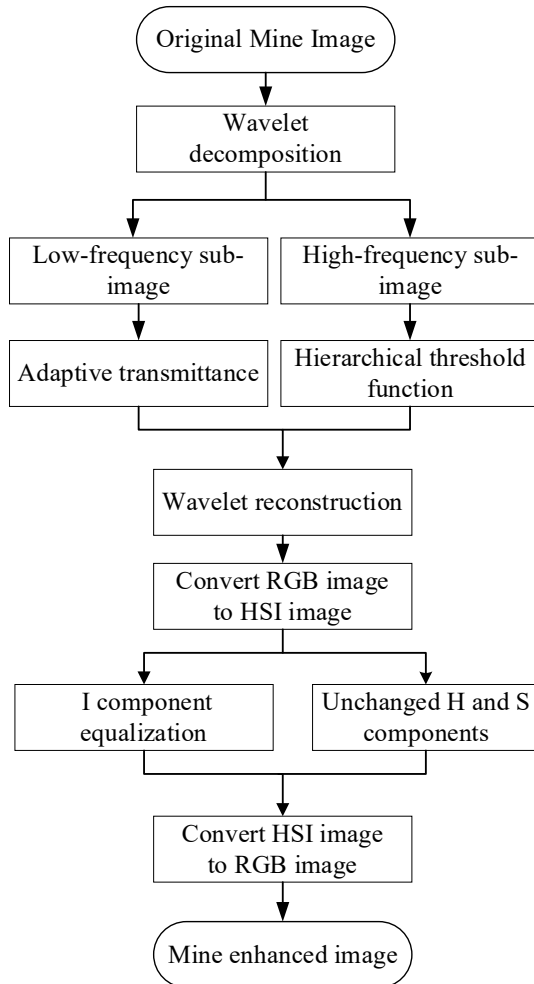


Fig. 5. Flow diagram of the proposed approach

Where M_{SE} is the mean square error.

Information entropy (IE) is employed to represent the amount of image information, and it is defined as follows.

$$IE(p) = -\sum_{i=0}^{255} p_i \log_2 p_i \quad (18)$$

Where p_i denotes the probability of occurrence of the i -th gray level.

The standard deviation (SD) is employed to reflect the dispersion of the image pixel value and the mean value. The greater SD value, the greater image contrast.

$$SD = \sqrt{\frac{1}{M \times N} \sum_{i=1}^M \sum_{j=1}^N (P(i, j) - \mu)^2} \quad (19)$$

Where $M \times N$ is the size of the image; $P(i, j)$ denotes the pixel value of the i -th row and j -th column, and μ represents the mean value.

The structural similarity index ($SSIM$) is utilized to measure the similarity between the dehazed image and original image. A higher $SSIM$ represents a smaller image distortion. It is defined as follows.

$$SSIM(x, y) = \frac{(2\mu_x \mu_y + C_1)(2\sigma_{xy} + C_2)}{(\mu_x^2 + \mu_y^2 + C_1)(\sigma_x^2 + \sigma_y^2 + C_2)} \quad (20)$$

Where μ_x and μ_y are the mean values of x and y , respectively; σ_x^2 and σ_y^2 are the variances of x and y ,

respectively; σ_{xy} represents the covariance of x and y ; C_1 and C_2 are constants that maintain stability.

A. Analysis of dehazing results

To verify the dehazing effect of the adaptive transmittance, two mine haze images are selected to compare the dark channel prior (DCP) algorithm [12] with the proposed algorithm. The comparison of the dehazing effect is shown in Fig.6.

Fig. 6 (b1) and (b2) show the dehazed image by DCP algorithm is overall dark, and the details are not clear. As seen from (c1) and (c2), the initial transmittance is optimized adaptively to suppress the generation of white halo blocks and make the edge details clearer. At the same time, the value of initial transmittance is reduced, and the overall image brightness is enhanced. Through I component equalization in HSI space, (d1) and (d2) are clearer than their corresponding reconstructed enhanced images (c1) and (c2). It is also can be seen from the corresponding gray histogram that the overall gray value of the original image is reduced, and the haze is suppressed effectively. Compared with the DCP algorithm, the proposed algorithm stretches the distribution range of the gray histogram and improves image contrast to some extent.

Table 1 presents that the time consumption of the proposed algorithm is shorter than that of the DCP algorithm. The proposed algorithm can complete the dehazing of the whole image by processing the low-frequency part. Compared with the DCP algorithm, both the dehazing effect and efficiency are improved by the adaptive transmittance optimization effectively.

TABLE I
COMPARISON OF THE RUNNING TIME BETWEEN THE TWO DEHAZING ALGORITHMS

Image	Running time/s	
	DCP algorithm	Proposed algorithm
Haze1	2.54	1.79
Haze2	2.60	1.83

B. Analysis of denoising results

Two mine roadway images will be employed to verify the denoising performance of the hierarchical threshold function in the high-frequency part. The noise variance estimation σ and IE are employed for the evaluation of the denoising effect. o_σ and o_{ie} represent σ and IE of the original image, respectively; $f_{RE,\sigma}$ and $f_{RE,ie}$ represent σ and IE processed by the proposed algorithm, respectively.

Fig. 7 shows the mine image processed by the proposed algorithm can retain the image edge information effectively while the image noise is suppressed. Table 2 presents that with the gradual increase of o_σ , the image noise processed by the proposed algorithm is stable in the range of 0.1-0.21, and the value of $f_{RE,ie}$ is basically unchanged. It is indicated that the proposed algorithm has a stable noise suppression effect and can maintain the edge details of the mine image effectively.

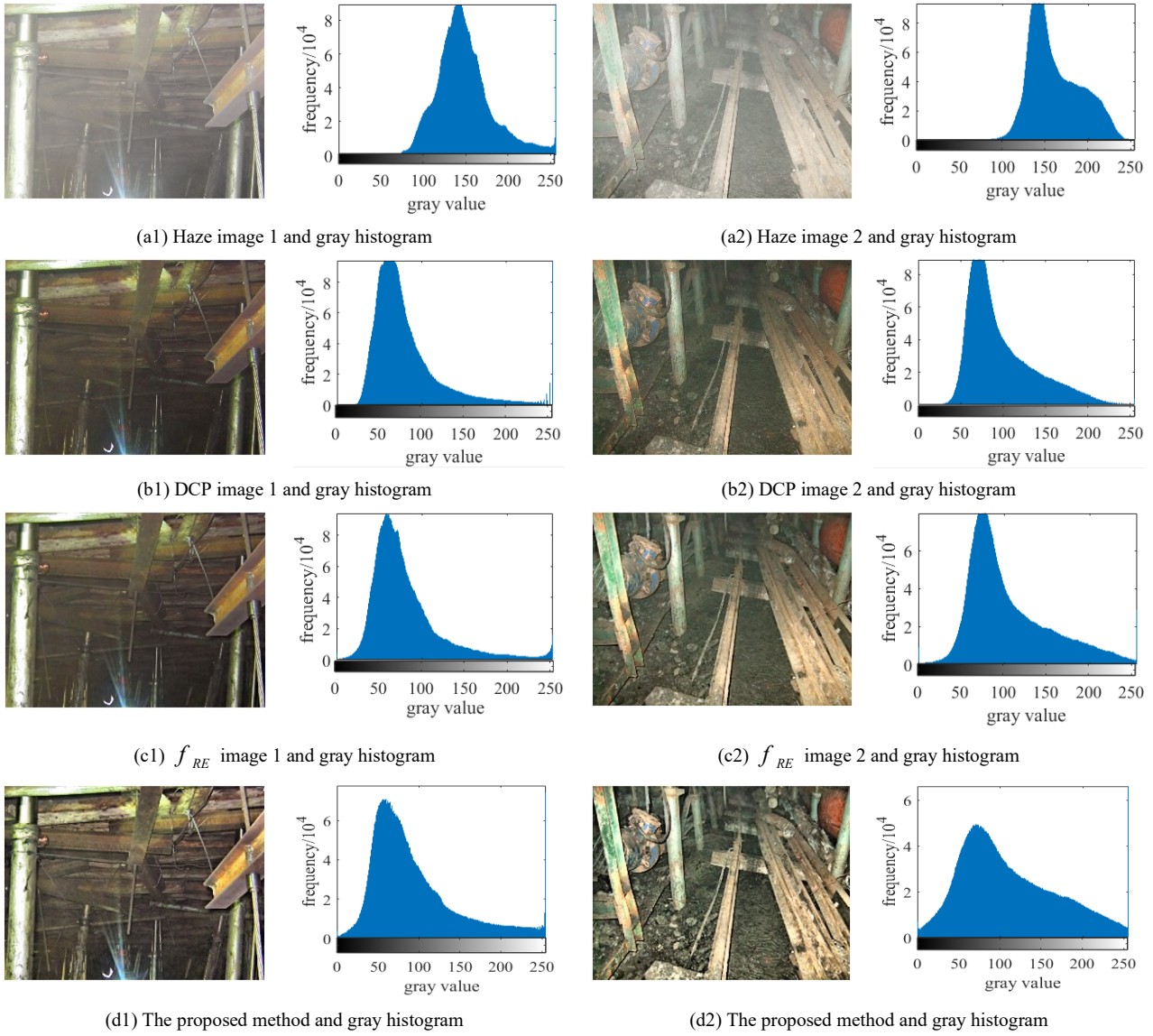


Fig. 6. Comparison of the dehazing effect



Fig. 7. Reconstructed enhanced images of roadway images

TABLE II
STATISTICS OF DENOISING EFFECT OF THE PROPOSED ALGORITHM

Image	O_{σ}	O_{ie}	$f_{RE,\sigma}$	$f_{RE,ie}$
roadway1	11.36	7.08	0.10	6.31
	15.89	7.13	0.14	6.32
	19.24	7.15	0.17	6.33
	21.98	7.16	0.20	6.33
roadway2	13.50	7.73	0.12	7.42
	17.35	7.72	0.16	7.43
	20.36	7.71	0.18	7.44
	22.98	7.71	0.21	7.45

To verify the denoising effect of the hierarchical threshold function, the two mine roadway images are added gaussian white noise with a mean value of 0 and a variance of 0.01. Meanwhile, the low-frequency coefficients are kept uniformly unchanged to ensure the accurate comparison of experimental results. The high-frequency coefficients are adopted by the soft threshold, hard threshold, literature [21], literature [22] and the proposed method, respectively.

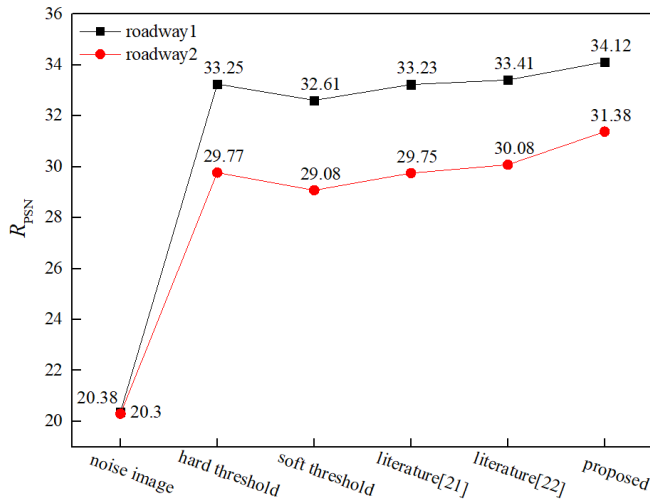


Fig. 8. Comparison of denoising indexes

Compared with the threshold function above, Fig. 8 shows hierarchical threshold function has a larger value of R_{PSN} , which has a better denoising effect. It is divided into three segments to estimate the wavelet coefficients, which can retain more high-frequency details and has an ideal denoising effect.

C. Analysis of comprehensive performance

To verify the overall enhancement performance of the proposed algorithm, the haze, dust and low illumination images are selected to compare and analyze the Contrast Limited Adaptive Histogram Equalization (CLAHE), Multiscale Retinex (MSR), MSRCR [25], DCP and the proposed algorithm. Fig. 9 presents the visual enhancement effect of each algorithm.

In Fig.9 (a), the original image is dark and has a poor visual effect and unclear image details. From Fig.9 (b) and (c), the images processed by CLAHE algorithm and MSR algorithm have higher brightness, but the overall image is white with severe color distortion. Besides, the haze image presents that both two algorithms have a halo phenomenon of different degrees. Fig.9 (d) shows the MSRCR algorithm has excellent color fidelity, and color deviation is eliminated basically. However, the enhanced details in the dark area are not obvious, and there is still a small amount of haze diffusion. Fig. 9 (e) shows that DCP algorithm can suppress the haze and dust of the mine test images. However, the overall brightness and contrast are low, and the enhanced image is not clear. From Fig.9 (f), the proposed approach can enhance the contrast and brightness significantly without color distortion, and the haze can be suppressed effectively to

avoid halo artifacts.

To objectively compare the overall enhancement effect of the five algorithms, Standard deviation (SD), Information entropy (IE), and Structural similarity index ($SSIM$) are selected as the quality evaluation indicators. The objective quality evaluation comparison of five algorithms is shown in Fig. 10.

In Fig. 10, the IE of the CLAHE and MSR algorithms are larger, but the SD and $SSIM$ are lower than that of the proposed algorithm. The two algorithms overexpose the brightness of mine images, so the enhanced images contain more information. However, the gray level of images is compressed, and image contrast is reduced. In addition, the enhanced image has serious color distortion. The color distortion is eliminated by MSRCR. But the SD and $SSIM$ of the MSRCR are lower in the haze and dust images. The algorithm does not enhance the details of dark areas, and there is a halo in bright areas. The haze and dust in the image can be suppressed effectively by DCP. However, the SD and IE values of DCP algorithm are low. The enhanced image is overall dark, which has a low image contrast and unclear image details. The proposed algorithm can suppress the halo artifact phenomenon and have high color fidelity. The overall objective evaluation indicators have been improved significantly, and the proposed algorithm achieves the highest value of SD and $SSIM$, outperforming the other four algorithms.

Combined with Fig. 9 and Fig. 10, we can see that the proposed algorithm avoids halo artifacts of the image by the adaptive transmittance optimization and reduces the overall transmittance value, which improves the image contrast and the overall dehazing effect. The wavelet coefficients are estimated in three segments by the hierarchical threshold function, which retains more image details and has a higher value of $SSIM$. The proposed algorithm has a better enhancement effect both on haze-dust and low-illumination image.

V. CONCLUSION

Aiming at the problems of halo blocks and detail loss existing in the enhanced mine images, an enhancement approach of the mine image based on adaptive transmittance and hierarchical threshold function is proposed. Firstly, in the low-frequency part, the position at the edge of field depth is determined adaptively, and the transmittance is optimized precisely. Then, the optimized transmittance is smoothed by guided filtering, which can retain the edge details and eliminate the white halo block. Next, the hierarchical threshold function is applied in the high-frequency part to estimate the wavelet coefficients, which can improve the denoising effect and retain more image details. Experimental results on several mine images show that the proposed approach can suppress the noise and haze and enhance the image details. Meanwhile, our proposed method has a better image contrast and is more suitable for mine image enhancement.

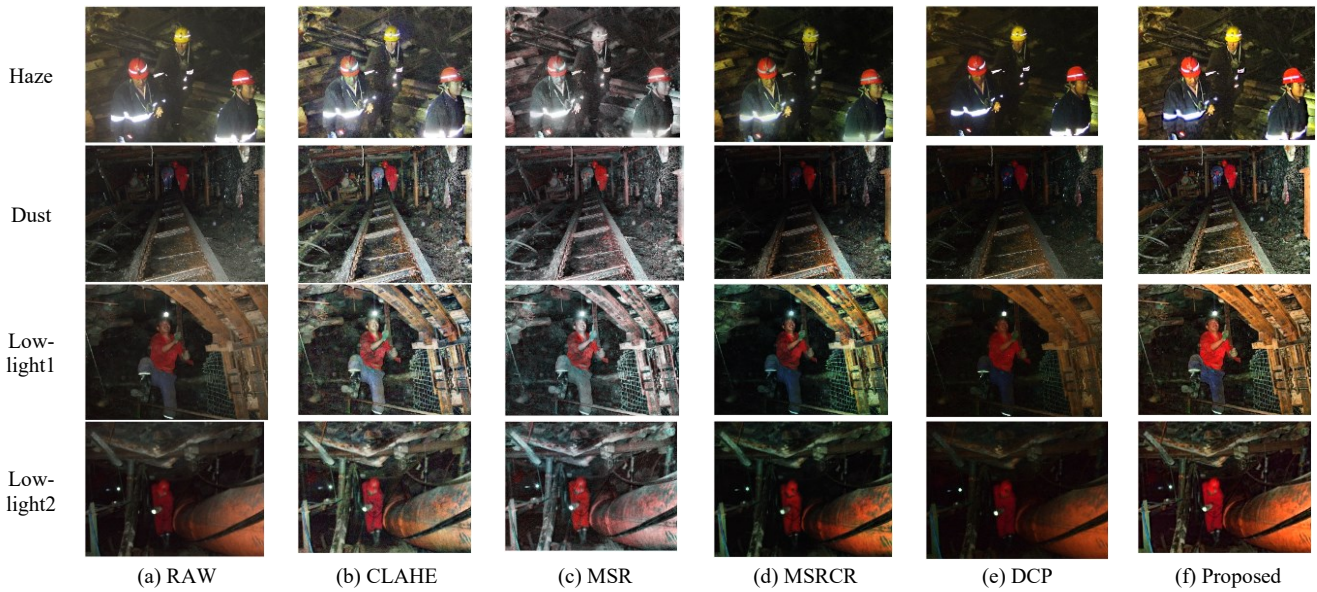
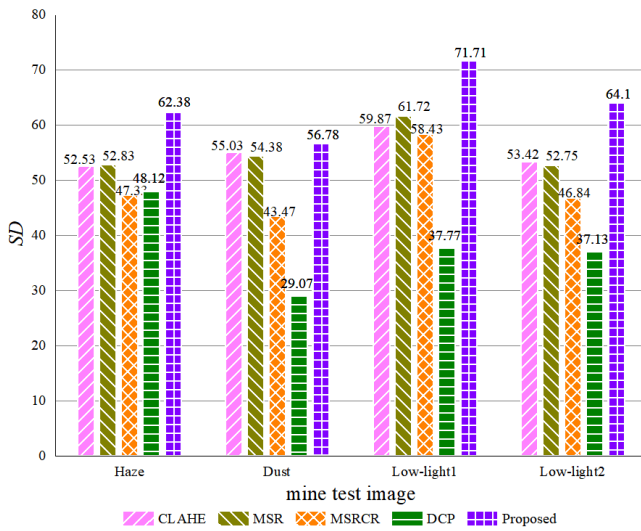
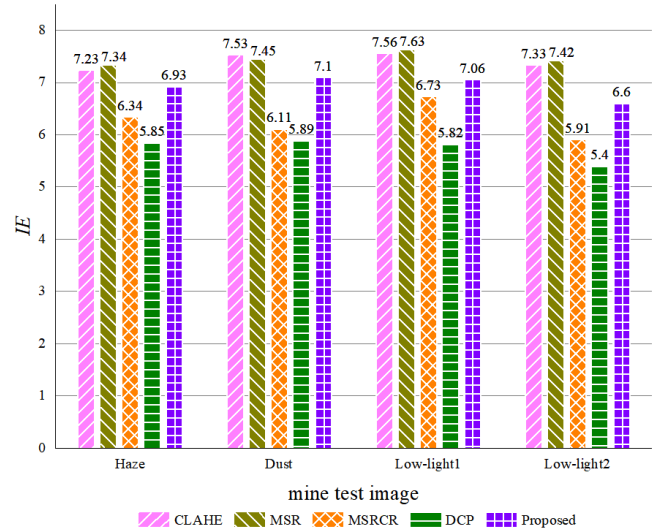


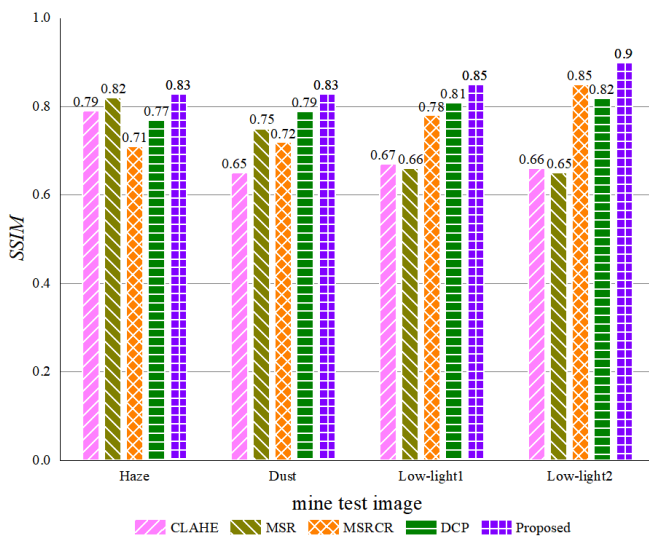
Fig. 9. Comparison of enhancement effects by different algorithms.



(a) SD



(b) IE



(c) SSIM

Fig. 10. Comparison of objective evaluation index

REFERENCES

- [1] Jiping Sun, "New technology and development of mine informatization and automation," *Coal Science and Technology*, vol. 44, no. 1, pp. 19-23+83, 2016.
- [2] Guofa Wang, Guorui Zhao, and Huaiwei Ren, "Analysis on key technologies of intelligent mining," *Journal of China Coal Society*, vol. 44, no. 1, pp. 34-41, 2019.
- [3] H F Yao, H Y Wang, and Y C Li, "Three-dimensional spatial and temporal distributions of dust in roadway tunneling," *International Journal of Mining Science and Technology*, vol. 7, no. 1, pp. 88-96, 2020.
- [4] M. Abdullah-Al-Wadud, M. Kabir, M. Dewan, and O. Chae, "A dynamic histogram equalization for image contrast enhancement," *IEEE Trans. on Consumer Electronics*, vol. 53, no. 2, pp. 593-600, 2007.
- [5] Dippel, M. Stahl, R. Wiemker, and T. Blaffert, "Multiscale contrast enhancement for radiographies: Laplacian Pyramid versus fast wavelet transform," *IEEE Trans Med Imaging*, vol. 21, no. 4, pp. 43-53, 2002.
- [6] J Xu, Y K Hou, and D W Ren, "STAR: A Structure and Texture Aware Retinex Model," *IEEE Transactions on Image Processing*, vol. 29, pp. 5022-5037, 2020.
- [7] Sim Kok Swee, Lim Choon Chen, and Tan Sin Ching, "Contrast Enhancement in Endoscopic Images Using Fusion Exposure Histogram Equalization," *Engineering Letters*, vol. 28, no. 3, pp. 715-723, 2020.
- [8] Liya Zhang, Bonan Hao, Qingyong Meng, Liang Wen, and Wenzhen Wu, "Method of image enhancement in coal mine based on improved

- retinex fusion algorithm in HSV space,” *Journal of China Coal Society*, vol. 45, no. 1, pp. 532–540, 2020.
- [9] Shoufeng Tang, Ke Shi, Guangming Tong, Jingcan shi, and Huashuo Li, “A mine low illumination image enhancement algorithm,” *Industry and Mine Automation*, vol. 47, no. 10, pp. 32–36, 2021.
- [10] C Y Li, J C Guo, and F Porikli, “LightenNet: a convolutional neural network for weakly illuminated image enhancement,” *Pattern Recognition Letters*, vol. 104, pp. 15–22, 2018.
- [11] C Wei, W Wang, and W Yang, “Deep retinex decomposition for low-light enhancement,” *arXiv:1808.04560*, 2018.
- [12] K M HE, J SUN, and X O TANG, “Single image haze removal using dark channel prior,” *IEEE Transactions on Pattern Analysis and Machine Intelligence*, vol. 33, no. 12 pp. 2341-2353, 2011.
- [13] K M HE, J SUN, and X O TANG, “Guided image filtering,” *IEEE Transactions on Pattern Analysis and Machine Intelligence*, vol. 35, no. 6 pp. 1397-1409, 2013.
- [14] Yingjie Mei, Yuan Ning, and Jinjun Chen, “Block-adjusted image enhancement algorithm combining dark channel prior with MSRCR,” *Acta Photonica Sinica*, vol. 48, no. 7 pp. 124-135, 2019.
- [15] Yong Chen, and Chentao Lu, “Single image dehazing based on super pixel segmentation combined with dark-bright channels,” *Laser and Optoelectronics Progress*, vol. 57, no. 16 pp. 239-247, 2020.
- [16] Xinyu Zhao, and Fuzhen Huang, “Image enhancement based on dual-channel prior and illumination map guided filtering,” *Laser and Optoelectronics Progress*, vol. 58, no. 8 pp. 53-62, 2021.
- [17] B L Cai, X M Xu, and K Jia, “DehazeNet: An end-to-end system for single image haze removal,” *IEEE Transactions on Image Processing*, vol. 25, no. 11 pp. 5187-5198, 2016.
- [18] B Y Li, X L Peng, and Z Y Wang, “AOD-Net: all-in-One dehazing network,” *IEEE International Conference on Computer Vision, Venice. IEEE*, pp. 4780-4788, 2017.
- [19] D CHEN, M HE, and Q FAN, “Gated context aggregation network for image dehazing and deraining,” *IEEE Winter Conference on Applications of Computer Vision (WACV). IEEE*, pp. 1375-1383, 2019.
- [20] Zijian Tian, Manli Wang, and Jun Wu, “Mine image enhancement algorithm based on dual domain decomposition,” *Acta Photonica Sinica*, vol. 48, no. 5 pp. 107-119, 2019.
- [21] X F Zhou, W W Zhu, and Q G Guo, “The denoising of ultrasonic signal based on asymptotic semi-soft thresholding function,” *Journal of Detection & Control*, vol. 33, no. 2 pp. 35-39, 2011.
- [22] Wenliang Jia, Yu Chen, and Qiang Chen, “Image denoising algorithm based on improved wavelet threshold,” *Microelectronics&Computer*, vol. 37, no. 10 pp. 24-29, 2020.
- [23] Weiqiang Fan, and Yi Liu, “Fuzzy enhancement algorithm of coal mine degradation image based on adaptive wavelet transform,” *Journal of China Coal Society*, vol. 45, no. 12 pp. 4248-4260, 2020.
- [24] Sreekala Kannoth, Sateesh Kumar H C, and Raja K B, "Denoising of Low Light Images using Patch Priors and Wavelets," *Engineering Letters*, vol. 29, no.3, pp. 1248-1263, 2021.
- [25] D J Jobson, Z Rahman, and Woodell G A, “A Multiscale Retinex for Bridging the Gap Between Color Images and the Human Observation of Scenes,” *IEEE Transactions on Image Processing*, vol. 6, no. 7 pp. 965-976, 1997.